



Contents lists available at ScienceDirect

Journal of Sound and Vibration

journal homepage: www.elsevier.com/locate/jsvi

An experimental study of sound generated by flows around cylinders of different cross-section

W.F. King¹, E. Pfizenmaier^{*,2}

Turbulenzforschung Berlin, Lotzestr. 14, D-12205 Berlin, Germany

ARTICLE INFO

Article history:

Received 18 June 2007

Received in revised form

15 July 2009

Accepted 30 July 2009

Handling Editor: P. Joseph

Available online 18 September 2009

ABSTRACT

The sound radiated by rigid cylinders placed transversely in a uniform stream has been measured in an anechoic wind tunnel over a range of Mach numbers ($M = 0.09–0.2$). The cylinders have different cross-sections, e.g., circular, square, rectangular, elliptic, and circular with lateral ribs or knurled surfaces. Different length to diameter ratios of the cylinders are also investigated. Results are presented as narrow band spectra, measured in the far field (acoustic as well as geometric). All spectra are presented with dimensionless (scaled) axes, as well as the original dimensional scales. It is shown that elliptic cross-sections are less noisy, compared to all other cylinders, but noise abatement techniques such as lateral ribs and knurled surfaces can also reduce tonal radiated noise. Two practical applications of these experiments are the reduction of radiated noise from pantographs of high-speed railway trains, and from the landing gear of modern passenger aircraft.

© 2009 Elsevier Ltd. All rights reserved.

1. Introduction

A slender solid body immersed in an ambient stream of moving fluid can generate tonal sound. This phenomenon, although known for millenia, was not subjected to scientific scrutiny until the latter half of the 19th century. In the late 1870s, Strouhal [1] published results of his experiments with vertical wires stretched taut between radial appendages of a frame affixed to a rotating shaft. His wires had diameters ranging between 0.18 and 8.5 mm, and each had a length of 490 mm. When the speed of the rotating wires exceeded some particular value, which was different for each wire, Strouhal observed audible tones. He called these sounds “friction tones” because he thought that they were caused by the drag (i.e., the friction) induced by the passage of air over the wires.

Shortly thereafter, Rayleigh [2] correctly determined that the wires within a stream of moving air vibrate in a direction transverse to that of the flow velocity and not in the direction of flow as Strouhal’s argument would suggest.

Since the time of these first experiments, there have been scores of reported investigations of the sound generated by the relative motion of a slender body immersed in an ambient fluid. However, it was not until Yudin [3] published the results of his studies of sound produced by rotating rods that it became generally accepted that sound could be generated without the body undergoing vibrational motion. The sound results from the interaction between the body and the fluid and is not dependent upon the body vibrating. A body capable of vibrating can, under certain circumstances, produce a

* Corresponding author. Tel.: +49 30 8111129.

E-mail address: epfizenmaier@t-online.de (E. Pfizenmaier).

¹ Deceased 2001.

² Formerly DLR-Abt. Turbulenzforschung Berlin; retired since 1996, now Lotzestr. 14, D-12205 Berlin, Germany.

higher intensity tone than when the body is rigid, but the sound-generating process per se is not dependent upon such vibrations.

Most of the investigations reported on since the late 1940s have involved a moving fluid interacting with a stationary cylinder having a circular cross-section. Very few studies have been carried out on cylinders having other cross-sections. Even for cylinders with a circular cross-section, the influence of many parameters on sound has not yet received much attention. Among such parameters are the ratio of the length of the cylinder to its diameter when the cylinder has a free end and the degree of roughness of the surface of a cylinder. The effect of these and other parameters on the fluid-mechanical aspects of cylinder-flow interactions have, however, been widely reported on, but the results of these studies do not always lend themselves to a direct interpretation of the possible aeroacoustical effects of the interactions. It is still not possible to perform an a priori prediction of the sound generated when a moving fluid interacts with a cylinder of arbitrary cross-section.

This statement is also valid today, if one looks onto analytical, computational and experimental work of the last decade. Nowhere in literature a comparative investigation on radiated noise from cylinders of different cross-sections is given.

A computation of vortex shedding and radiated sound for a circular cylinder is given by Cox et al. [4]. They use also “the Lighthill acoustic analogy” combined with Reynolds-averaged Navier–Stokes flow computations, to predict the tonal noise, generated by vortex shedding from a circular cylinder for a range of Reynolds-numbers from $100 < Re < 5 \times 10^6$. They report on results for the mean drag, mean pressure coefficient, Strouhal numbers and fluctuating lift in comparison to experiments. The computed flow field is used as an input for the noise prediction. Both the noise amplitude and frequency agree well with experiments, if an appropriate correlation length for the vortex shedding is introduced in the turbulence model. Part of this work should be comparable to our experimental results.

Another investigation from Pérot et al. [5] deals with “a computation of the noise, generated by low Mach number flows around a cylinder” obviously a circular cylinder, “and a wall-mounted half-cylinder.” Regarding only a half-cylinder is due to developments for modern cars, where “aerodynamic noise is becoming the major source of annoyance”. An estimation of broadband noise at Mach number flows of about $M \approx 0.1$ is considered, applying a “two-step method combining incompressible CFD-calculations with the acoustic analogy”. The half-cylinder is used to simulate a simplified side-mirror shape of a car and its noise radiation. So only the full cylinder results may be comparable to our data.

An analytical study of flow induced cylinder noise is reported by Gloerfelt et al. [6]. They formulate the problem as “a diffraction problem at solid non-vibrating surfaces for low Mach numbers, according to the classical aeroacoustic papers by Powell, Ffowcs-Williams, Crighton and Howe”. A numerical illustration but no comparison to experiments is involved and the results are also restricted to the case of circular cylinders. Only two papers could be found in the publications of the last decade which are concerned with the noise radiation of square cylinders. Tosh et al. [7] report on “the prediction of noise, radiated by flow over a smooth-square cylinder, where computations of turbulent flow over a bluff body and the resulting acoustic signature are performed. The near-field turbulent flow is coupled to the far-field acoustic prediction model of Ffowcs-Williams and Hawkings,” but again a comparison to our results seems difficult. The second paper on a similar topic is given by Inoue et al. [8]. They regard the “sound generated by two square cylinders placed in a side-by-side arrangement, in a uniform flow”, as it is the situation at the contact strips of a real railway pantograph. Since in this report we only regard single cylinders, results could be better compared to one of our earlier papers, where we investigated the sound emission of complete railway pantographs. But these results are only documented in internal reports and not as yet published [9,10]. Other papers in the last decade are concerned p.e. with landing gear noise, where also flow structures around circular cylinders but in a tandem arrangement radiate noise. This is reported by Jenkins et al. [11]. But only information on the flow field is given, in order to “better understand the mechanisms associated with component interaction noise” and no comparison to our measurements is possible.

At last an early report on “Low-speed drag of cylinders of various shapes” by Delany and Sorensen [12] may be mentioned. This report describes aerodynamic measurements on drag coefficients and Strouhal numbers of cylinders of various shapes, where also circular, quadratic, rectangular, triangular and elliptic cylinders are investigated. The Strouhal numbers they measured in the flow field of cylinders with comparable dimensions are similar to the Strouhal numbers in our aeroacoustic measurements.

One of the purposes of the investigations discussed in the present report is to provide at least a modicum of data on sound generated by flows around cylinders having various cross-sections and ratios of length to diameter. Another purpose is to study relatively simple ways of abating this sound. In several countries, high-speed tracked vehicles now carry passengers at speeds over 250 km/h. At such speeds, aerodynamically generated sound becomes a significant component of wayside noise levels. One of the aerodynamic sound sources on a high-speed electric train is caused by flows around the pantograph. Since a pantograph comprises a number of slender bodies, the results obtained from studies of cylinder noise should be useful in helping to abate pantograph noise.

Descriptions of (i) the open-jet wind tunnel in which measurements were made, (ii) the cylinder models, and (iii) the arrangement of the models in the test section of the wind tunnel are given in Section 2. Section 3 contains a general comment on the results of the measurements, the background noise, and some of the problems encountered during the tests.

Detailed discussions of the results for the various cylinders are given in Sections 4–6. Results of the measurements of sound generated by circular cylinders are treated in Section 4. Section 5 comprises an analysis of results for square and rectangular cylinders, while Section 6 deals with sound generated by elliptic cylinders.

Two techniques for reducing the level of sound generated by flows around circular cylinders were tested. Data stemming from these measurements are shortly mentioned in Section 7. Finally, a brief summary of the more significant results is given in Section 8 along with a short list of the still unanswered questions concerning cylinder noise and its abatement.

2. Facility, models, measuring equipment, and test arrangements

2.1. Facility

The investigations were carried out in the acoustic wind tunnel (AWB) located on the grounds of the DLR Research Center in Braunschweig. A drawing of this facility is given in Fig. 1. As shown in the figure, an anechoic chamber surrounds the test section of the open jet. The exit nozzle has a rectangular cross-section of height 1.2 m and width of 0.8 m. With this nozzle, the wind tunnel has a peak operating wind speed of 69 m/s. At all wind speeds used during the present investigations, the turbulence level in the jet core was below about 0.5 percent.

2.2. Models

For ease in identifying the various models, each was given a code name consisting of letters and numbers. These code names, a brief description and a sketch of each model are listed in Table 1. Unless otherwise noted, all cylinder models have one free end and a smooth surface. All cylinders in the experiments are fixed with their length axis perpendicular to the flow. A cylinder having a circular cross-section is referred to as a circular cylinder, one with a square cross-section is a square cylinder, etc.

In most cases, the brief descriptions of each cylinder model in Table 1 should be sufficient to identify the model and its significant characteristics. An important parameter that cannot be listed in the table is the aspect ratio of the cylinder. The aspect ratio is the length of the cylinder divided by its frontal dimension. For a circular cylinder, its frontal dimension is its diameter. The aspect ratio of each model will be given when the results of the measurements are discussed.

Cylinders for which the descriptions in Table 1 are not sufficient are FAm and FBm. Drawings of the “F” models are also given in Table 1.

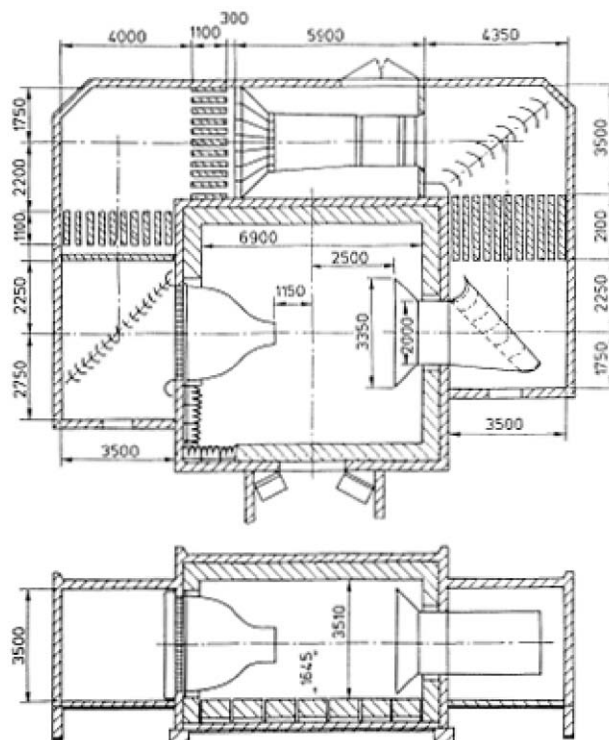


Fig. 1. Acoustical wind tunnel (AWB) located in the DLR Research Center in Braunschweig. Dimensions are in mm.

Table 1
Code names, descriptions, and illustrations of models.

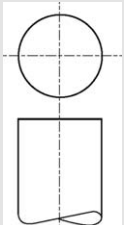
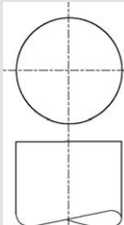
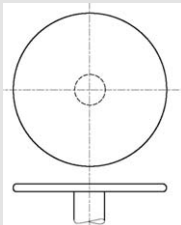
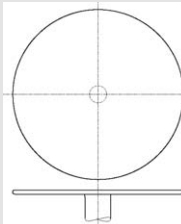
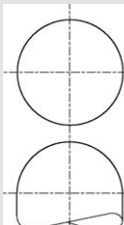
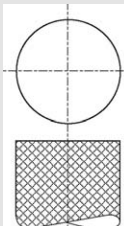
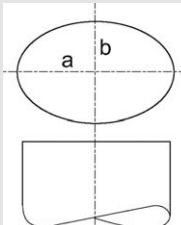
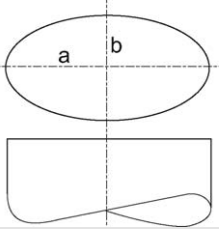
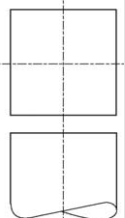
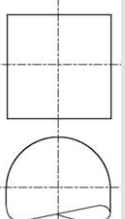
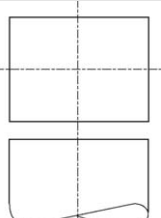
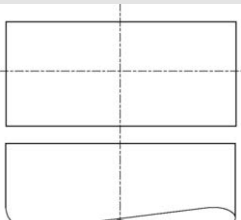
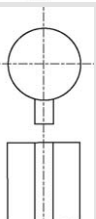
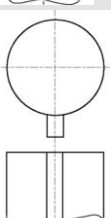
Model	Description	Illustration
A1	Circular cylinder, 20 mm diameter	
A2	Circular cylinder, 30 mm diameter	
A1P	Circular cylinder, 20 mm diameter with 100 mm diameter circular end plate	
A1P3	Circular cylinder, 20 mm diameter with 200 mm diameter circular end plate	
A2R	Circular cylinder, 30 mm diameter with rounded free end	
AK	Circular cylinder with knurled surface, 30 mm diameter	
C1	Short elliptic cylinder, $2a = 42$ mm, $2b = 29$ mm; $b/a = 0.69$	

Table 1 (continued)

Model	Description	Illustration
C2	Long elliptic cylinder, $2a = 58$ mm, $2b = 30$ mm; $b/a = 0.517$	
D	Square cylinder, 30×30 mm cross-section, flow velocity normal to face	
DR	Like D except that free end is rounded	
E1	Rectangular cylinder with $B/d = 1.31$ where $B =$ downstream dimension and $d =$ frontal dimension transverse to the flow, $d = 30$ mm	
E2	Rectangular cylinder with $B/d = 2.2$ and $d = 30$ mm	
FAM	Circular cylinder, 20 mm diameter, rectangular rib attached to one side, $m = 5$ mm equals the transverse dimension of the rib	
FBm	Circular cylinder, 30 mm diameter, rectangular rib attached to one side, $m = 5$ mm equals the transverse dimension of the rib	

Unless otherwise noted, all models have a smooth surface.

As shown in Table 1, the models FAm and FBm have a lateral rectangular rib attached to one side of a circular cylinder. With respect to the direction of flow, the rib has a frontal dimension of w . The important parameter for characterizing sound abatement is the ratio w/D , where D is the diameter of the circular cylinder. Models having two different diameters were tested, namely $D = 20$ mm (FAm) and $D = 30$ mm (FBm). The letter m denotes the frontal dimension of the rib in mm.

2.3. Measuring equipment and test arrangements

2.3.1. Measuring equipment

Sound measurements were made with two Brüel & Kjaer $\frac{1}{4}$ -in condenser microphones, model 4135. In order to suppress wind noise, each microphone was fitted with a sponge rubber wind screen. Signals were first preamplified with Brüel & Kjaer preamplifiers, model 2633, and then fed via shielded cable to Brüel & Kjaer amplifiers, model 2610. Signals were stored on a Tascam DA88 8-channel digital tape recorder which has a fixed sampling frequency of 48 kHz. On-site analysis of the data was carried out with a Hewlett-Packard HP 3567A FFT analyzer and a PC.

Test runs in the wind tunnel for every model were carried out during a running time of about 5 min in order to allow an integration time which is long enough to stabilize the collected data.

2.3.2. Test arrangements

“Far” and “near” measurement positions: For most of the measurements, the cylinders were mounted in a vise-like fixture that was bolted onto a table. The table was rigidly fixed onto the grating that formed the floor in the test section of the wind tunnel. A drawing of this arrangement is illustrated in Fig. 2. The distance between the top of the table and the lower edge of the jet nozzle was $d_E = 350$ mm, and the height d_F of the vise-like fixture was 190 mm. As indicated in the figure, cylinders were positioned at a downstream distance of $x_N = 1100$ mm from the nozzle edge. At the location of the cylinder, the core flow in the jet was at a height d_c of about 120 mm above the lower edge of the nozzle, or about 470 mm above the table. The length of cylinder under investigation is denoted by L . In order to ensure that L was fully within the core flow, we let $d_c = 140$ mm, i.e., $d_T = 490$ mm (see Fig. 2). The length L depended upon the particular investigation at hand. In order to suppress sound generated by vortex shedding from the portion of the cylinder below L , or below d_T , we wrapped this part of the model with rough (K40) emery cloth.

All cylinders were positioned along the centerline of the jet, as indicated in the upstream view in Fig. 3 and the top view in Fig. 4. Sound was measured with two microphones labeled No. 1 and No. 2. Microphone No. 1 was positioned on the far side of the jet, while microphone No. 2 was on the near side. The designations “far” and “near” refer to the proximity of the region to the door leading into the test section. The heights of the microphones above the grating were selected to coincide with the midpoint of the particular cylinder being studied. In most cases, both lateral distances R_1 and R_2 between the centerline of the model (or of the jet) and the microphones were 1.4 m (see Fig. 4), under 90° to the center of the model.

A photograph of a circular cylinder mounted as described above is shown in Fig. 5. To ensure that no unwanted sound from either reflections or as a consequence of flow interactions with the shear layer would contaminate the results, a thick sheet of sponge rubber was draped over the table and mounting fixture and held in place with cloth belts (see Fig. 5).

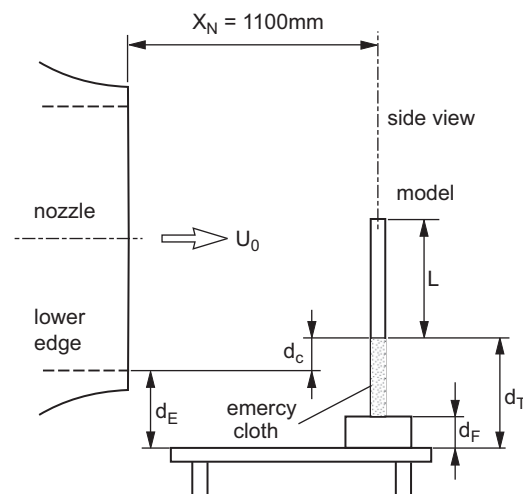


Fig. 2. Arrangement of cylinders in test section of wind tunnel (side view).

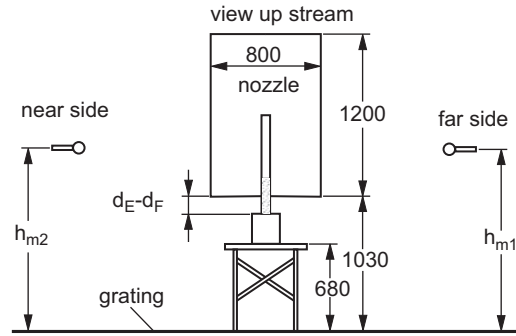


Fig. 3. Arrangement of cylinders in test section of wind tunnel (upstream view).

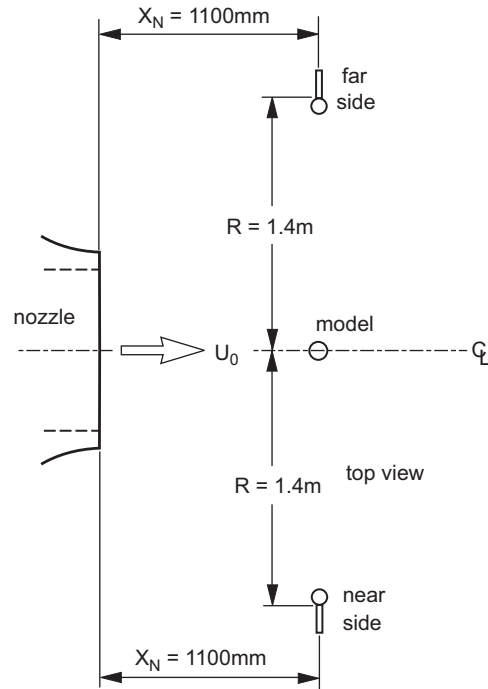


Fig. 4. Arrangement of cylinders in test section of wind tunnel (top view). Model distance to nozzle exit equals X_N .

3. General comments on measurements and results

3.1. Sound-pressure levels and spectra

Unless otherwise indicated, all sound-pressure levels listed in Sections 4–7 are unweighted linear levels for the frequency range 100–1000 Hz.

The decibel scale on the left hand side ordinate of each figure is labeled with the abbreviation SPL (sound-pressure level), whereas in the body of the text, in figure captions, and in equations, the abbreviation L_p denotes sound-pressure level.

3.2. The power spectral density (PSD)

Second scales are added in most of the narrow-band spectra; the frequency-axis is completed with a Strouhal number scale, and the SPL-axis is completed by a power spectral density (PSD) scale, which is labeled as \log_{10} PSD. Logarithmic values of PSD are related to the base 10; but to shorten the plot, only \log PSD is given. Definition and tables for SPL and PSD values are given in the Appendix.

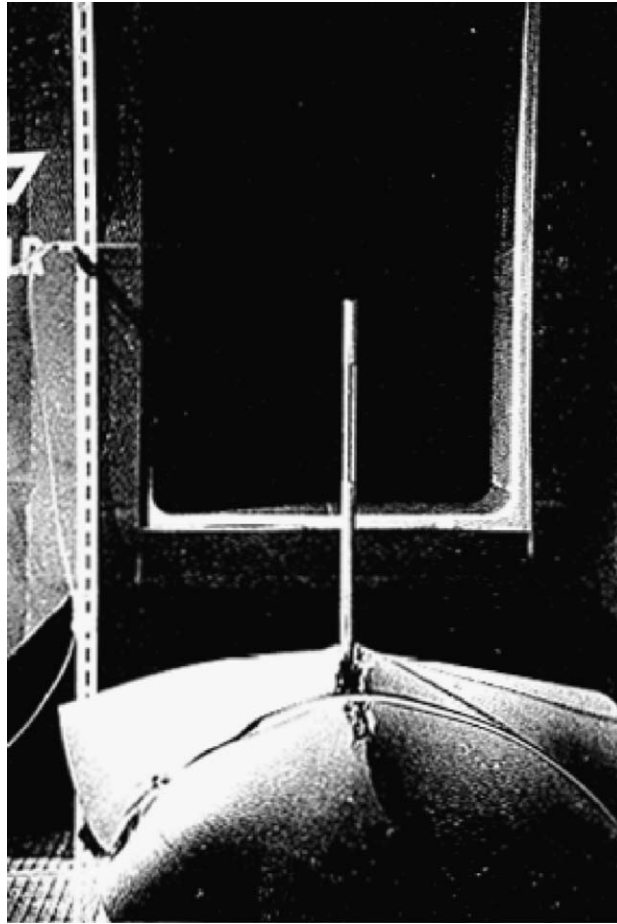


Fig. 5. Upstream view of circular cylinder mounted on test table covered with sponge-rubber mat.

3.3. Control of far-field conditions for microphone locations

Microphones were positioned in a distance of $R = 1.4$ m to the sound sources behind the cylinders. We then have to judge two conditions for the acoustical and the geometrical far field. Both conditions are met for all measurements, except only for some cases of square and rectangular cylinders, where $R/\lambda < 1$ for the peak Strouhal number. Therefore the acoustical far-field condition is not met, but in all cases the geometrical far-field condition is obtained.

3.4. Background noise

Background noise is defined as the sound generated by the airflow when all mounting fixtures, including the mats of sponge rubber used to inhibit both vortex shedding and reflections, are positioned in the test section without the model. The appropriate background noise has been removed from all narrow-band spectra shown in Sections 4–7. Wherever possible, the frequency range for the spectra is 100–1000 Hz. In a number of cases, however, the signal level within the lower part of the frequency range lies so close to the level of the background noise that when the latter is subtracted from the signal, the resulting curve is essentially meaningless. When this situation occurs, the affected spectrum has a low-frequency cut-off above 100 Hz.

4. Results for circular cylinders

4.1. Cylinders with one free end

4.1.1. Effect of aspect ratio on sound

The aspect ratio of a circular cylinder immersed in a moving fluid is one of the most important parameters for establishing its sound-pressure level and Strouhal number. To quantify the effect of aspect ratio, we measured sound

Table 2

Effect of aspect ratio on sound-pressure levels and Strouhal numbers generated by model A1 circular cylinder having a diameter of 20 mm.

L/D	U_0 (m/s)	L_p (dB)	f_0 (Hz)	S_D
2	48	75.7	–	–
3	64	81.6	–	–
4	48	75.5	326	0.136
6	48	76.2	364	0.152
9	64	84.0	540	0.169
9	64	84.7	554	0.173
10	48	79.6	420	0.175
10	64	85.7	–	–
12	64	85.6	–	–
12	64	85.8	558	0.174
15	48	81.6	436	0.182
15	64	86.6	566	0.177
15	64	87.1	586	0.183
15	32	71.0	292	0.183
15	64	87.1	586	0.183
15	48	82.9	460	0.192
17	64	90.8	596	0.186
17.5	64	90.1	598	0.187
20	64	92.5	602	0.188
25	32	83.2	318	0.194
25	49	94.8	480	0.196
25	54	96.2	518	0.192
25	64	98.0	616	0.193
25	69	101.2	666	0.193
30	49	96.1	480	0.196
30	64	100.5	608	0.190
35	32	83.8	308	0.193
35	55	98.2	526	0.191
35	64	102.3	608	0.190

Frequency range is 100–1000 Hz, and the distance between the models and microphone was $R = 1.4$ m; $R/L \geq 2$. L_p is given as an overall sound-pressure level (OASPL) integrated over all frequencies.

generated by flows around a number of model A1 cylinders having aspect ratios ranging from 2 to 35. The results of these measurements are listed in Table 2. This table shows that L_p rises clearly with the aspect ratio L/D . One example may be depicted: $L/D = 3$ at $U_0 = 64$ m/s gives $L_p = 81.6$ dB, whereas $L/D = 30$ at $U_0 = 64$ m/s rises to 100.3 dB.

4.1.2. Narrow band spectra and Strouhal numbers

Narrow-band spectra of sound generated by model A1 are given in Fig. 6 for aspect ratios of 3, 9, and 15 and in Fig. 7 for aspect ratios of 15, 20, and 25. In addition to the rise in peak spectral level as L/D becomes larger, the peak frequency also increases as aspect ratio increases. The rate of increase of peak frequency decreases, however, at the higher aspect ratios. As can be seen in Fig. 7, the difference in the values of the peak frequencies at $L/D = 20$ and 25 is very slight. Similar spectra for A1 at aspect ratios of 25, 30, and 35 are plotted in Fig. 8. Except for minor variations due to experimental scatter, the results in this figure show that the values of the peak frequencies at these aspect ratios remain essentially constant. At $L/D = 30$ and 35, however, a second, lower frequency peak now appears in the spectra. The value of this second peak frequency at $L/D = 35$ is 577 Hz which yields a Strouhal number of 0.180. When this Strouhal number is compared with others in Table 2 it can be seen that a Strouhal number of 0.180 is typically generated by a cylinder having an aspect ratio of about 15.

End effects play an important role in establishing both the Strouhal number and sound-pressure level when the cylinder has a free end and the aspect ratio is not high. In the vicinity of the free end, the value of the coefficient of fluctuating lift can be up to three times higher than it is on the rest of the cylinder, and the flow is three dimensional. Some investigators (see [13]) suggest that the aspect ratio should be about 45 to ensure that the consequences of end effects become insignificant. Having said this, we still do not know why end effects appear to be absent from the spectrum in Fig. 7 at $L/D = 25$ but clearly make their appearance in Fig. 8 at $L/D = 35$.

Strouhal numbers for the A1 cylinder are plotted in Fig. 9 as a function of aspect ratio. The Reynolds number and Mach number for each series of measurements are also listed in the figure. All of the Strouhal numbers were measured at subcritical Reynolds numbers. Within this range there appears to be no influence of Reynolds number on the results. The three different Strouhal numbers reported by Farivar [14] could not be observed for low aspect ratio ($L/D < 12$) free-ended cylinders. One should note that Farivar's results are for fluid-dynamical measurements not acoustical ones. The values of the Strouhal numbers listed in Table 2 and in Fig. 9 represent results based upon frequencies of the peak spectral levels. Secondary peak frequencies such as that in Fig. 8 for $L/D = 35$ are not listed in the tables nor shown in Fig. 9 unless these secondary peaks become dominant. Peak Strouhal numbers are denominated in all figures of narrow band spectra by S_p .

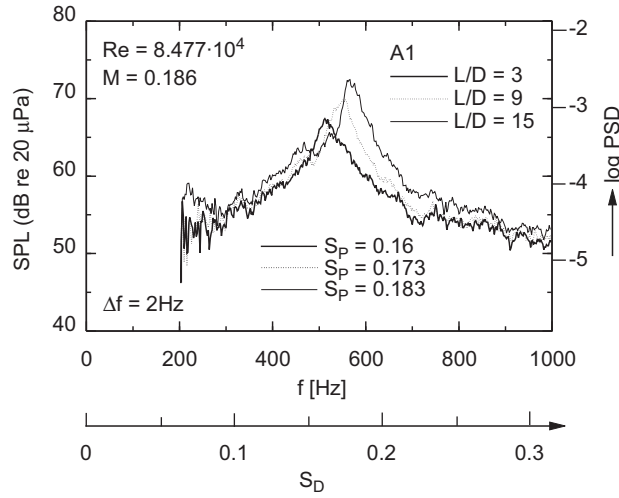


Fig. 6. Circular cylinder A1; narrow band spectra; $R/D = 70$; $R/\lambda > 1$; $R/L > 1$.

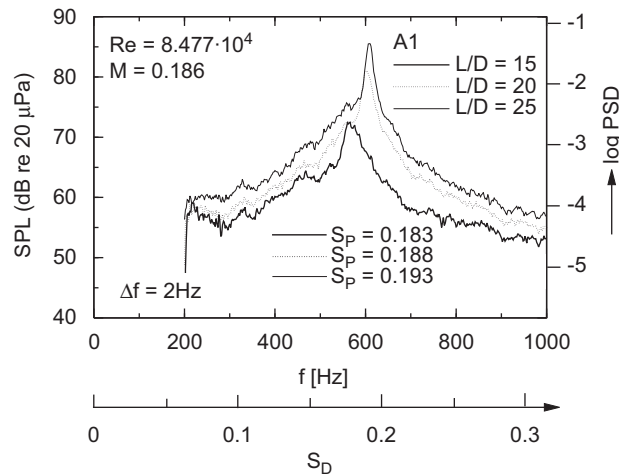


Fig. 7. Circular cylinder A1; narrow band spectra; $R/D = 70$; $R/\lambda > 1$; $R/L > 1$.

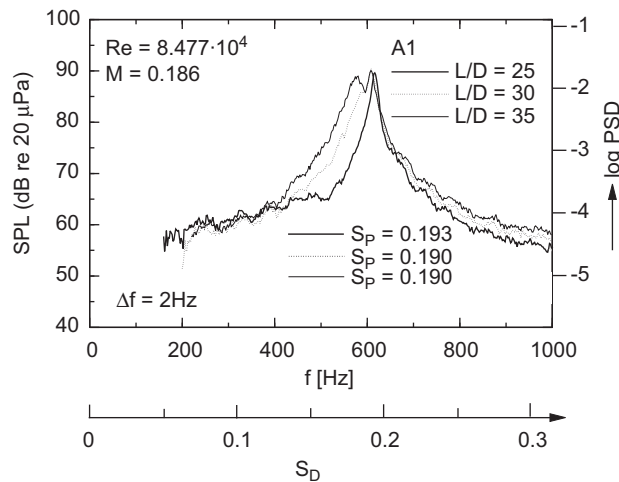


Fig. 8. Circular cylinder A1; narrow band spectra; $R/D = 70$; $R/\lambda > 1$; $R/L > 1$.

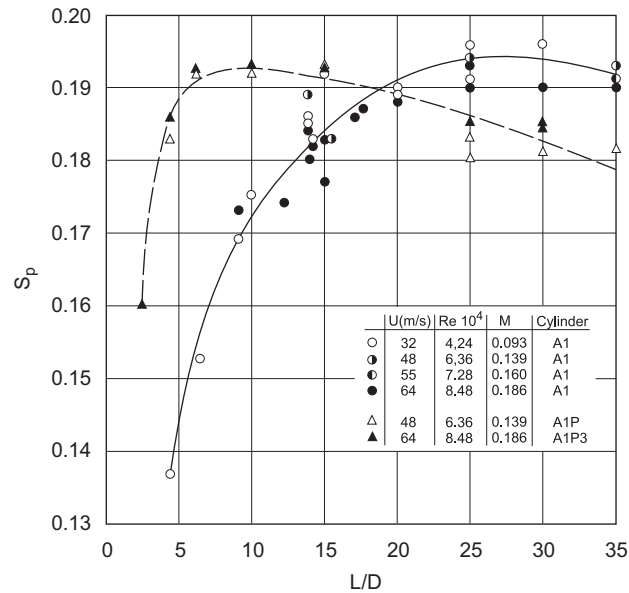


Fig. 9. Strouhal number S_p as a function of aspect ratio L/D . S_p , peak Strouhal number. Comparison for circular cylinder A1 and circular cylinder A1P and A1P3 with circular endplate A1P = 100 mm diameter, A1P3 = 200 mm diameter. See Section 2.2, Table 1.

A circular cylinder with an essentially infinite aspect ratio has a Strouhal number lying between 0.19 and 0.20 at subcritical Reynolds numbers. The results in Fig. 9 clearly demonstrate that one effect of low aspect ratio is to lower the Strouhal number. At an aspect ratio of 5, the Strouhal number is nearly 30 percent less than it is at $L/D = 25$.

4.2. Cylinders with a circular end plate

Cylinders with a circular end plate are given in Table 1, labeled A1P and A1P3. The effect of the aspect ratio on the Strouhal numbers for those cylinders has also been investigated. Summarizing results are given in Fig. 9. Here the Strouhal number decreases for aspect ratios > 10 .

5. Results for square and rectangular cylinders

The results of measurements for the DR, D, E1, and E2 models are listed in Table 3. For comparison, the results for corresponding circular cylinders are also given in the table. As in the previous tables, the peak frequencies and Strouhal numbers in Table 3 refer to the highest peak spectral levels. Since the peak frequencies for the square and rectangular cylinders were expected to be low, the microphone was positioned at a lateral distance of 2.5 m from the cylinders to avoid near-field effects. The results for the sound-pressure levels given in Table 3 as well as for the narrow-band spectra discussed below were subsequently rescaled for a microphone distance of $R = 1.4$ m. These transformations were made to facilitate comparisons with results actually measured at a distance of $R = 1.4$ m from the models.

The angle of attack of the flow velocity impinging upon the 30 mm-wide face of either the square or rectangular cylinder was 0° , i.e., the 30 mm-wide faces were perpendicular to the flow velocity. Both square and rectangular cylinders have a relatively long correlation length, when compared with circular cylinders. The flow always separates along the fixed straight edges of a square or rectangular cylinder. Consequently, the correlation lengths are longer than for a corresponding circular cylinder. In addition, these parameters are not strongly dependent upon Reynolds number. But there was no possibility to quantify the correlation length for rectangular cylinders, compared to the correlation length for circular cylinders, in these experiments.

5.1. Narrow band spectra and Strouhal numbers

5.1.1. Square cylinders

Narrow-band spectra of sound produced by the DR cylinder at an aspect ratio of 16.7 and the D cylinder at an aspect ratio of 25 are superposed in Fig. 10. The spectral level of the secondary peak in the D spectrum is lower than the corresponding peak in the DR spectrum although the level of the primary peak for the D model is about 5 dB higher than the analogous peak for the DR model. End effects are obviously enhanced by the rounded free end on the DR model. The Strouhal numbers of the primary peaks are 0.119 for the DR model and 0.122 for the D model. The aspect ratio of a square

Table 3
Sound generated by square and rectangular cylinders.

Model	U_0 (m/s)	L/D	L_p (dB)	f_0 (Hz)	S_D	Δ (dB)
A2R	32	16.7	75.7	202	0.189	–
DR	32	16.7	86.2	128	0.120	10.5
A2R	48	16.7	86.3	298	0.186	–
DR	48	16.7	94.2	190	0.119	7.9
A2R	67	16.7	94.0	412	0.184	–
DR	67	16.7	102.6	262	0.117	8.6
A2	67	16.7	93.0	409	0.183	–
D	67	16.7	102.4	262	0.117	9.4
A2	49	25	94.9	312	0.191	–
D	49	25	101.5	200	0.122	6.6
A2	64	25	99.4	406	0.190	–
D	64	25	109.0	258	0.121	9.6
E1	48	16.7	95.0	164	0.103	8.7
E1	67	16.7	101.1	232	0.104	8.1
E2	48	16.7	94.5	114	0.071	8.2
E2	67	16.7	103.1	160	0.072	10.1

Frequency range is 100–1000 Hz, and the distance between the models and microphone was $R = 1.4$ m. For comparison, values for corresponding circular cylinders are also given. Legend: $\Delta = L_p$ of model minus L_p of corresponding circular cylinder. S_D corresponds to S_p in the figures of the narrow band spectra.

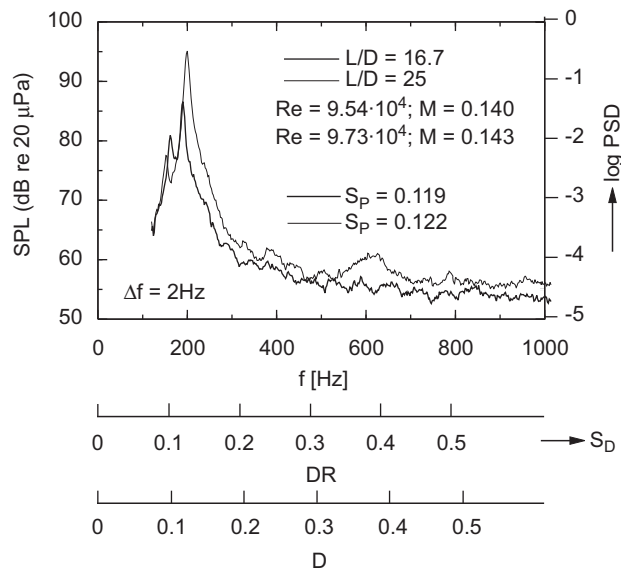


Fig. 10. Square cylinders D, DR; narrow band spectra; $R/D = 46.6$; $R/\lambda > 1$; $R/L > 1$.

cylinder does not have as strong an influence on the Strouhal number as does the aspect ratio of a circular cylinder (see Tables 2 and 3). Any further discussion of results for the D model should be postponed until Section 6.3 where the acoustic properties of square, circular, and elliptic cylinders are compared. Because of the slightly different Re and M numbers in Fig. 10 there should be a double scale for the PSD-values. But since the difference due to Re and M is very small, the upper and lower values of PSD are indicated by broadening the PSD marks a bit, compared to the other narrow band spectra. The upper limit of the respective mark corresponds to the lower Re and M values and vice versa.

5.1.2. Rectangular cylinders

As defined in Table 1, the E1 rectangular cylinder has a ratio of its downstream dimension B to its cross-stream dimension d of 1.31. A narrow-band spectrum of sound generated by the E1 model is compared with a spectrum for the A2 circular cylinder in Fig. 11. Both cylinders have an aspect ratio of 16.7. The rectangular cylinder produces two well defined spectral peaks with the primary one having a Strouhal number of 0.104 while the secondary one has a Strouhal number of 0.087. At some value of the ratio B/d , the downstream dimension of a rectangular cylinder is large enough so that the airflow that separated from the cylinder on the upstream edges will reattach to the sides of the cylinder and separate again.

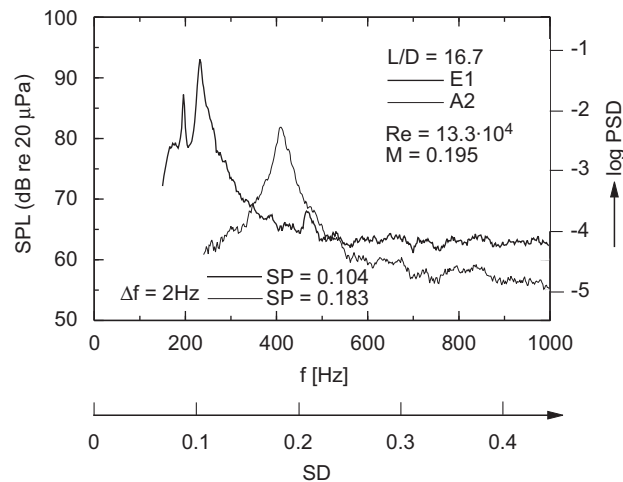


Fig. 11. Rectangular cylinder E1; narrow band spectra; $R/D = 46.6$, $R/\lambda > 1$, $R/L > 1$.

This process produces two vortex-shedding frequencies and hence two acoustical frequencies. The lower-frequency peak in the E1 spectrum may be caused by the process just described, or it may be produced by end effects. There was not sufficient time to make enough measurements of sound generated by rectangular cylinders to be able to definitively decide which of these two possibilities occurred. In so far the description is somewhat speculative. If the flow reattaches prior to the cylinder's rear end, this initial separation may not cause any periodic flow phenomena. Additional aerodynamic insight is necessary to clarify the relevant noise generating mechanism.

The spectral level of the primary peak in the spectrum for E1 is over 10 dB higher than the peak level due to the A2 model which has the same aspect ratio and frontal dimension as the rectangular cylinder. Even the secondary peak in the spectrum for the E1 model has a level that is 6 dB higher than the peak level for the circular cylinder. As indicated in Table 3, the overall sound-pressure level produced by the E1 cylinder is 8.1 dB higher than the corresponding level generated by the A2 cylinder.

As listed in Table 3, the primary spectral peak for the E2 model at $U_0 = 67$ m/s has a Strouhal number of 0.072 while for the E2 model, at $U_0 = 48$ m/s the value is 0.071. No measurements at lower wind tunnel speeds were made for either the E1 or E2 cylinders because of the very low peak frequencies involved.

5.2. Sound-pressure levels and speed exponents

5.2.1. Sound-pressure levels

Sound-pressure levels generated by both square and rectangular cylinders are higher than levels produced by corresponding circular cylinders at the same flow speed. The differences in sound-pressure levels between a square or rectangular cylinder and a corresponding circular one are indicated by Δ in Table 3.

5.2.2. Speed exponents

Over the range of flow speeds represented by the results in Table 3, small differences in sound-pressure levels have a strong effect on the value of the speed exponent. To compensate for the inevitable scatter in sound-pressure levels (scatter on the order of tenths of a decibel), it is desirable to have a relatively large number of results available. For the square and rectangular cylinders, the set of data is very small, and the resulting values for the speed exponents should be viewed as tentative values.

The average of the three possible combinations of speed exponents for the DR model at an aspect ratio of 16.7 is 5.1, whereas for the D model at $L/D = 25$, the speed exponent has a value of 6.4. For the rectangular cylinders, the E1 model exhibits a speed exponent of 4.2, while the value for the E2 model is 5.9. Most of these speed exponents therefore indicate the dipole-character of these sound sources.

6. Results for elliptic cylinders

The measured results for the elliptic cylinders are collected in Table 4. The aspect ratio for these cylinders is arbitrarily defined as the ratio of their length to their frontal dimension which for the C1 model is 29 mm and for the C2 model is 30 mm. For some purposes it could be more appropriate to use the streamwise dimension of each cylinder as the denominator in the aspect ratio, but this possibility is ignored in the present report.

Table 4 also lists some appropriate results for circular cylinders whose frontal dimension is essentially the same as that for the elliptic cylinders. The difference in sound-pressure levels between an elliptic cylinder and the corresponding circular one is denoted by Δ . When Δ is negative, the elliptic cylinder generates the lower level.

The major axis of an elliptic cross-section is denoted by “2a”, while its minor axis is labeled “2b”. Each of the elliptic cylinders was positioned in the test section so that the major axis of the ellipse was parallel to the freestream velocity.

In order to facilitate comparisons of results for the C1, C2, A2 and D cylinders, the frontal dimension of the last three models is 30 mm. Because the elliptic cylinders came from commercially available stock, it was necessary to settle for a frontal dimension of 29 mm for the C1 model. The ratio b/a of this model is 0.69, while that for the C2 cylinder is 0.517 (see Section 2.2, Table 1).

6.1. Narrow band spectra and Strouhal numbers

A comparison of spectra for the C1 and A2 cylinders is shown in Fig. 12 where the aspect ratio for both cylinders is 16.7. At this lower aspect ratio, the level of the spectral peak produced by the C1 cylinder is about 7 dB lower than the corresponding peak generated by the A2 cylinder. End effects play a more important role at this aspect ratio than they do at one of 25. The Strouhal number for the peak frequency produced by the circular cylinder is 0.185, and, as we have discussed

Table 4
Sound-pressure levels and Strouhal numbers generated by elliptic cylinders.

Model	U_0 (m/s)	L/D	L_p (dB)	f_0 (Hz)	S_D	Δ (dB)
A2	32	16.7	74.6	200	0.188	–
C1	32	16.7	72.7	225	0.204	–1.9
C2	32	16.7	77.5	258	0.242	2.9
A2	48	16.7	85.4	296	0.185	–
C1	48	16.7	83.5	332	0.201	–1.9
C2	48	16.7	86.4	382	0.239	1.0
A2	67	16.7	93.0	409	0.183	–
C1	67	16.7	91.7	464	0.201	–0.7
C2	67	16.7	90.0	909	0.407	–3.0
A2	32	25	85.4	206	0.193	–
C1	32	25	75.4	234	0.212	–10.0
A2	49	25	94.9	312	0.191	–
C1	49	25	85.6	360	0.213	–9.3
C2	49	25	92.0	534	0.327	–2.9
A2	64	25	99.4	406	0.190	–
C1	64	25	92.2	468	0.212	–7.2
C2	64	25	102.5	798	0.374	3.1

Frequency range is 100–1000 Hz, and the distance between the models and microphone was 1.4 m. For comparison, results for corresponding circular cylinders are also listed. Legend: $\Delta = L_p$ of model minus L_p of corresponding circular cylinder. The ratio b/a of the C1 cylinder is 0.69 while that of the C2 cylinder is 0.517. S_D corresponds to S_p in the narrow band spectra.

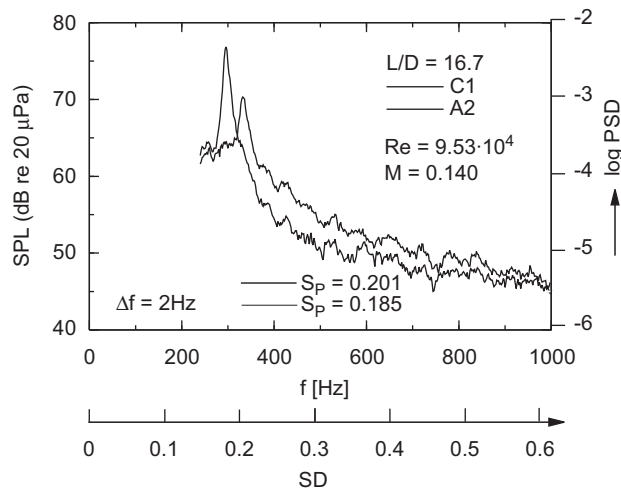


Fig. 12. Elliptic cylinder C1 and circular cylinder A2; narrow band spectra; $R/D = 46.6$, $R/\lambda > 1$, $R/L > 1$.

above, the corresponding value for the elliptic cylinder is 0.201. These slightly lower Strouhal numbers and smaller difference between the peak spectral levels are consequences of end effects.

The upper bound of the subcritical range of Reynolds numbers depends upon the ratio b/a of the particular cylinder as well as upon the streamwise dimension. Except for a few papers, e.g., those of Modi and Dikshit [15] and Modi and Wiland [16], there is a paucity of publications in the open literature on the fluid dynamical and acoustical properties of elliptic cylinders. For example, there was no data on critical Reynolds numbers for elliptic cylinders. On the basis of the acoustical results, the critical Reynolds number for the C2 cylinder appears to lie somewhere between 1.2×10^5 and 1.8×10^5 , as discussed below, but it cannot be specified any closer than this. For the C1 cylinder, the critical Reynolds number lies above 2×10^5 .

Narrow-band spectra of sound generated by the short C1 and long C2 elliptic cylinders are superposed in Fig. 13. Both cylinders have an aspect ratio of 16.7. At the flow speed of 67 m/s and a Reynolds number of 1.33×10^5 , the flow over the C2 cylinder is in the critical regime. A simple indication that the flow is critical is provided by the Strouhal number for this cylinder which is 0.407 (see Table 4). On the other hand, the flow over the C1 cylinder is clearly still subcritical at a Reynolds number of 1.29×10^5 . The Strouhal number corresponding to the peak frequency for the C1 model is 0.201.

A different relationship between the spectra is obtained when the aspect ratio of both cylinders is 25. Narrow-band spectra of sound produced by the C1 and C2 elliptic cylinders are superposed in Fig. 14. With a Strouhal number of 0.374, the spectral peak for the C2 cylinder again indicates that the flow is in the critical regime, but the peak is more clearly defined than it is in Fig. 13 where the aspect ratio is 16.7. In Fig. 13 the overall sound-pressure level for the C2 cylinder is

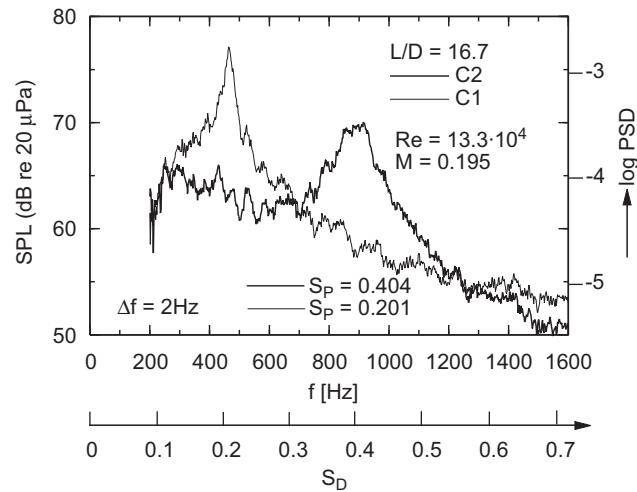


Fig. 13. Elliptic cylinders C1 and C2; narrow band spectra; $R/D = 46.6$, $R/\lambda > 1$, $R/L > 1$. C1 $\rightarrow b/a = 29/42 = 0.69$, C2 $\rightarrow b/a = 30/58 = 0.517$, see Table 1.

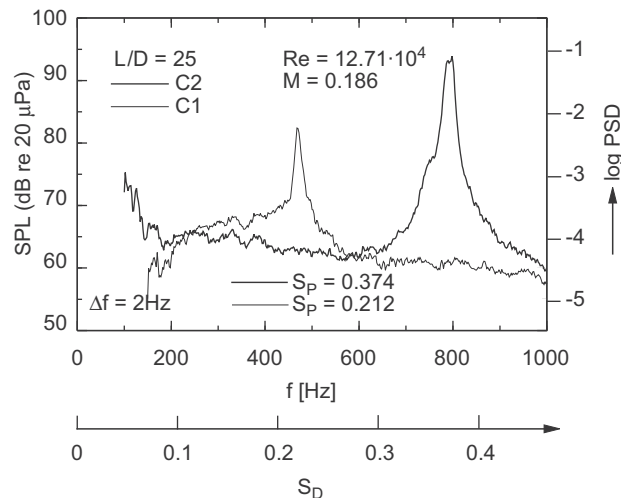


Fig. 14. Elliptic cylinders C1 and C2; narrow band spectra; $R/D = 46.6$, $R/\lambda > 1$, $R/L > 1$.

90.0 dB and for the C1 cylinder it is 91.7 dB (see Table 4). The C1 cylinder generates a higher sound-pressure level than does the C2 cylinder when each has an aspect ratio of 16.7. In Fig. 14, where the aspect ratio is 25, the C2 cylinder produces an overall sound-pressure level of 102.5 dB, while the level of the C1 model is only 92.2 dB (see Table 4). At the higher aspect ratio, the C2 model has become the louder cylinder. This phenomenon is a result of end effects which are more pronounced at lower aspect ratios.

6.2. Sound-pressure levels

As can be seen in Table 4, the sound-pressure levels generated by the C1 cylinder are lower than the levels produced by the A2 cylinder, regardless of whether the aspect ratio is 16.7 or 25. This difference in sound-pressure levels is, however, much larger at an aspect ratio of 25 than it is at 16.7. At still lower aspect ratios, it seems likely that the progressively stronger influence of end effects will cause the levels produced by both cylinders to become more similar.

Sound-pressure levels generated by the C2 model are lower than the levels produced by the corresponding circular cylinder at some aspect ratios and speeds and higher at others. At an aspect ratio of 25 and $U_0 = 49$ m/s, for example, the sound-pressure level produced by the C2 cylinder is, according to Table 4, 2.9 dB lower than the corresponding level due to the A2 circular cylinder, while the sound-pressure level generated by the C2 elliptic cylinder is 3.1 dB higher than the level produced by the equivalent circular cylinder at $U_0 = 64$ m/s.

For smooth circular cylinders, the critical Reynolds number is about 3×10^5 . For smooth elliptic cylinders, the critical Reynolds number has a lower value which depends upon the ratio b/a and streamwise dimension, as is discussed in Section 6.1. The ratio b/a of an elliptic cylinder is also instrumental in determining the sound-pressure level generated by the cylinder. Because the aeroacoustical properties of two elliptic cylinders were investigated only, the functional relationship between ratio b/a and sound-pressure level is not known. Whether the relatively high sound-pressure level produced by the C2 elliptic cylinder is due to its ratio b/a , its Reynolds number or its relatively large streamwise dimension is unknown at present. More investigations will have to be undertaken before these questions can be answered. Such future studies should be concerned with establishing the influence of ratio b/a , aspect ratio, and Reynolds number on radiated noise levels.

6.3. Comparison of sound-pressure levels generated by elliptic, circular, and square cylinders

Narrow-band spectra of sound generated by the A2 circular cylinder, the C1 elliptic cylinder, and the D square cylinder are superposed in Fig. 15. All cylinders have an aspect ratio of 25. As could be expected from the results already discussed, the peak spectral level for the square cylinder is about 7 dB higher than the corresponding level due to the circular cylinder and about 15 dB higher than the equivalent level for the elliptic cylinder. The broadband higher-frequency sound-pressure levels produced by both the square and elliptic cylinders are 3–5 dB higher than the corresponding levels due to the circular cylinder. For the band levels used for the spectra, however, the broadband noise levels are at least 10 dB lower than the spectral peak in each spectrum.

Overall sound-pressure levels for these three cylinders are plotted in Fig. 16 as a function of flow speed and of Reynolds and Mach number. If low sound-pressure levels are a design parameter for equipment subjected to moving air, the results

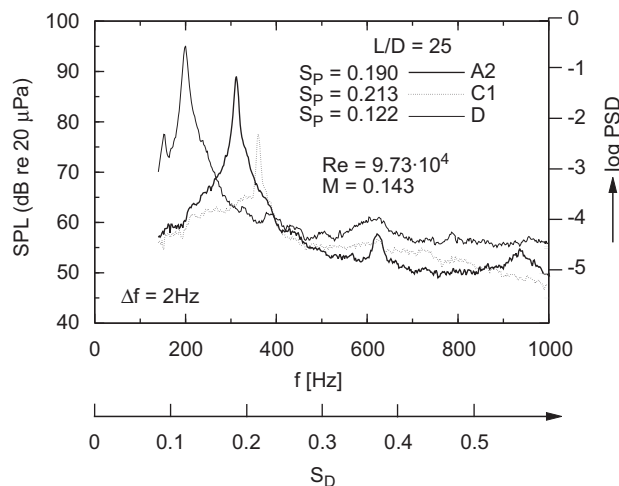


Fig. 15. Comparison of the narrow band spectra for A2, C1 and D cylinder.

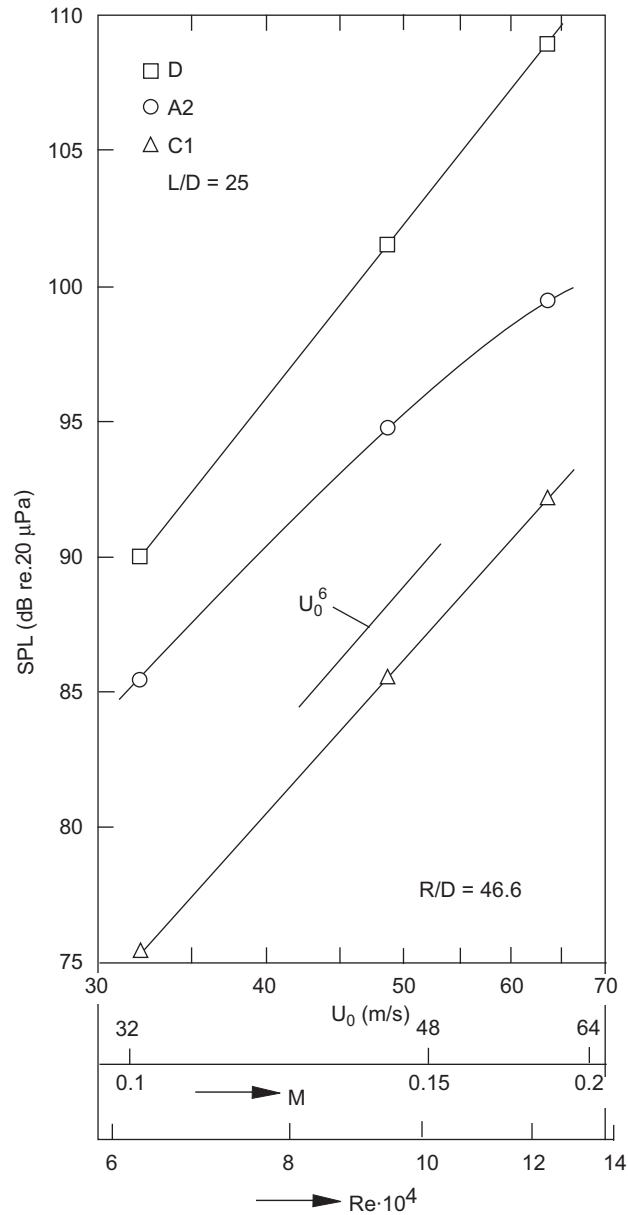


Fig. 16. Comparison of sound-pressure levels generated by the D square cylinder, the A2 circular cylinder and the C1 elliptic cylinder; $L/D = 25$ for all; $R/\lambda > 1$; $R/L > 1$.

in Fig. 16 clearly demonstrate the inherent advantage of the C1 elliptic cylinder. Sound-pressure levels produced by the circular cylinder are about 9 dB higher than those associated with the C1 elliptic cylinder under comparable conditions.

As is already discussed above, the results in this section for the elliptic cylinder pertain only to the C1 model with its ratio b/a of 0.69 and maximum Reynolds numbers of 1.33×10^5 . Fig. 16 indicates again that all sorts of cylinders, be they circular, square, rectangular or even elliptic, behave similar to acoustical dipoles in radiating sound proportional to U_0^6 .

7. Sound abatement techniques

Two techniques to reduce sound radiated by cylinders in flows were also investigated, namely

1. a lateral rib as indicated in Table 1 and labeled FAm and FBm and
2. enlarging the surface roughness as shown in Table 1 in the model AK with knurled surface.

Both methods reduce the radiated sound, especially single tones dramatically. Splitter plates in the rear of the cylinders, a usual method to avoid coherent vortex shedding, have not been tested because of the lack of time and because lateral ribs proved to be an optimal device to be realized at electrical pantographs.

8. Concluding remarks and summary

When a uniform, low-turbulence flow of fluid interacts with a cylinder whose aspect ratio is essentially infinite, the flow is two-dimensional and vortex shedding occurs in what might be called a classical manner. This situation occurs, for example, when the wind interacts with high-tension overhead wires. When the aspect ratio of a cylinder is finite and low, and a free end is exposed to the airstream, three-dimensional flow conditions predominate over a significant fraction of the span. At low enough aspect ratios, the flow can be three-dimensional over the entire cylinder. The consequences of three-dimensional flow are usually referred to as end effects. Most of the investigations of flow past cylinders reported on in the literature involve cylinders whose aspect ratio is less than 20. There is no free end, however, because these studies are typically carried out in the closed test-section of a wind tunnel with the cylinder spanning the distance from one wall to another. The influence of the walls stabilizes the flow, and the results of measurements are similar (but not always identical) to those that would be obtained with essentially infinite cylinders.

In the acoustical studies of sound generated by circular cylinders with one free end, it was found that the value of the aspect ratio is an important property for establishing both the Strouhal number of the peak frequency and sound-pressure level. As its value increases, the influence of the aspect ratio on these parameters decreases. At an aspect ratio of about 25, its influence, albeit still noticeable, is no longer a dominant factor in establishing the values of the acoustical parameters.

When the free end of a circular cylinder terminates in a circular end plate having a diameter of from 5 to 10 times that of the cylinder, the flow in the vicinity of the free end becomes more two dimensional, i.e., like the flow over the rest of the cylinder, and end effects in the classical sense cease to exist. As is discussed in the text, the Strouhal numbers listed in the tables are formed with the frequencies of the spectral peak having the highest level in each spectrum. In Fig. 9 where the results for circular cylinders with an end plate are given, the values of most Strouhal numbers for cylinders whose aspect ratio is 25 or larger are lower than would ordinarily be expected. The spectra of sound generated by these cylinders have two peak frequencies with the level of the lower-frequency peak generally being higher than the level of the other peak. The mechanism leading to the frequency shift is still an open problem, however.

Measurements of sound generated by elliptic and square cylinders were made at only two aspect ratios, viz., 16.7 and 25. Since there are no obvious differences in the values of the Strouhal number for square cylinders at the two aspect ratios, end effects apparently play a smaller role here than they do for circular cylinders. The Strouhal numbers for the short elliptic cylinder C1 are, however, obviously a little bit lower at an aspect ratio of 16.7 than they are at one of 25. For the long cylinder C2 yet they are lower at $L/D = 16.7$ ($Re = 6.36 \times 10^4$ to 9.53×10^4) than for $L/D = 25$ ($Re = 9.73 \times 10^4$ to 12.7×10^4), as well as higher. This is confusing and not explained. Since no measurements of sound produced by an elliptic cylinder were made at aspect ratios larger than 25, it is not known how higher values of the aspect ratio affect sound generated by these cylinders.

For the same value of aspect ratio and frontal dimension, sound-pressure levels generated by a square cylinder are from 6 to 10 dB higher than the corresponding levels produced by a circular cylinder, while sound-pressure levels generated by the C1 elliptic cylinder are about 10 dB lower than the corresponding ones due to the circular cylinder. Sound-pressure levels produced by the C2 elliptic cylinder proved to be about as high as, or, in some cases, higher than, the corresponding level generated by a circular cylinder. These results indicate the need to know the functional relationship between sound-pressure level and the ratio b/a for elliptic cylinders. It would indeed be fortuitous if the ratio b/a of the semi-minor axis and the semi-major axis of the C1 cylinder was optimal in terms of a low noise design.

Two different methods of abating sound generated by circular cylinders were investigated. One method involves attaching an auxiliary rectangular rib onto one side of a cylinder. For a rib of width w and cylinder of diameter D , the results show that the reduction of sound-pressure level is a function of both the ratio w/D and the aspect ratio. At an aspect ratio of 16.7 and a value of 0.33 for w/D , the sound-pressure level reduction is 9.7 dB. These results appear to be independent of Reynolds number.

The second method for abating sound-pressure levels involves the use of surface roughness to force the laminar boundary layer on the cylinder to undergo transition to turbulence. The surface of a 30 mm-diameter cylinder was roughened by knurling it in such a way that the surface was covered with 0.5 mm-high pyramidal protuberances. The results of the measurements indicate that sound abatement by roughness is a function of aspect ratio. As is the case with end effects, the aspect ratio probably ceases to be an important property of the cylinder at values of 25 and higher. Fluid mechanical studies indicate that the height of the roughness element is an important parameter for inducing the boundary layer to undergo transition to turbulence. The radiated noise level generated by a cylinder is no doubt also a function of the roughness height. We suspect that roughness elements having a smaller height than the 0.5 mm-high pyramidal protuberances on our AK model would yield a much higher level of sound abatement at high flow speeds. These results are mentioned shortly in Section 7.

The results of the investigations designed to abate radiated noise levels generated by slender bodies point the way towards further studies that could yield even greater reductions in sound-pressure levels as described by King [17] and the

original internal report, which gives more details of the measurements is cited as [18]. In this report a survey on the experts literature about aerodynamic data of cylinders with different cross-sections up to 1996 is given.

Acknowledgments

This study was part of an experimental investigation of pantograph noise which was commissioned by the Deutsche Bundesbahn in 1996.

We should like to thank the Akustik Data Engineering Office for its support of the work described in this report. The assistance provided by the staff members of the AWB wind tunnel is also acknowledged.

Many thanks are also due to Dr. M. Hermann and Dipl. Ing. L. Neuhaus for their help to collect and store the experimental data.

We also wish to thank Prof. C. Morfey (ISVR) for his proposals to modify and shorten the text. A further acknowledgement goes to Dipl. Math. Matthias Pfizenmaier and Evelyn Kulzer for providing the TEX-files and the figures of this report.

Appendix A. Definition of the power spectral density (PSD)

$$\text{PSD} = \left(\frac{p}{\rho U_0^2} \right)^2 \left(\frac{R}{D} \right)^2 \frac{U_0}{\Delta f D} = \frac{p^2}{\rho^2 U_0^3} \frac{R^2}{D^3} \frac{1}{\Delta f}$$

where $p^2 = p_0^2 \cdot 10^{\text{SPL}/10}$; $p_0 = 20 \mu\text{Pa}$, ρ is the density of air in kg/m^3 , U_0 the mean wind tunnel velocity in m/s , R the distance of the microphones to the sound source in m , D the diameter of cylinder in m , Δf the band width of narrow-band filter in $1/\text{s}$, ρU_0^2 the dynamic head in N/m^2 , $(R/D)^2$ the distance scaling, $U_0/\Delta f D$ the the reciprocal of a Strouhal number, based on the bandwidth Δf .

Appendix B. Tables

Transformation of sound-pressure levels to power spectral densities with a distance scaling is shown in Table B1. Wind tunnel velocities and corresponding Mach and Reynolds numbers in the narrow band spectra in Table B2.

Table B1

Transformation of sound-pressure levels (SPL) to power spectral densities (PSD) according to equation in Appendix A with a distance scaling $(R/D)^2$.

\log_{10} PSD	PSD	SPL (dB re 20 μPa)					
		$U_0 = 32 \text{ m/s}$	$U_0 = 48 \text{ m/s}$	$U_0 = 49 \text{ m/s}$	$U_0 = 55 \text{ m/s}$	$U_0 = 64 \text{ m/s}$	$U_0 = 67 \text{ m/s}$
<i>D = 0.02 m</i>							
-7	10^{-7}	19.9	25.2	25.4	26.9	28.9	29.5
-6	10^{-6}	29.9	35.2	35.4	36.9	38.9	39.5
-5	10^{-5}	39.9	45.2	45.4	46.9	48.9	49.5
-4	10^{-4}	49.9	55.2	55.4	56.9	58.9	59.5
-3	10^{-3}	59.9	65.2	65.4	66.9	68.9	69.5
-2	10^{-2}	69.9	75.2	75.4	76.9	78.9	79.5
-1	10^{-1}	79.9	85.2	85.4	86.9	88.9	89.5
0	1	89.9	95.2	95.4	96.9	98.9	99.5
1	10	99.9	105.2	105.4	106.9	108.9	109.5
2	100	109.9	115.2	115.4	116.9	118.9	119.5
<i>D = 0.03 m</i>							
-7	10^{-7}	25.2	30.4	30.7	32.2	34.2	34.8
-6	10^{-6}	35.2	40.4	40.7	42.2	44.2	44.8
-5	10^{-5}	45.2	50.4	50.7	52.2	54.2	54.8
-4	10^{-4}	55.2	60.4	60.7	62.2	64.2	64.8
-3	10^{-3}	65.2	70.4	70.7	72.2	74.2	74.8
-2	10^{-2}	75.2	80.4	80.7	82.2	84.2	84.8
-1	10^{-1}	85.2	90.4	90.7	92.2	94.2	94.8
0	1	95.2	100.4	100.7	102.2	104.2	104.8
1	10	105.2	110.4	110.7	112.2	114.2	114.8
2	100	115.2	120.4	120.7	122.2	124.2	124.8

All PSD values are given in a logarithmic plot to the basis 10.

Table B2

Wind tunnel velocities U_0 and corresponding Mach and Reynolds numbers in the narrow band spectra; $Re = U_0(D/\nu)$, $\nu = 15.1 \times 10^{-6} \text{ m}^2/\text{s}$, $a = 343.3 \text{ m/s}$.

Nr.	D (m)	U_0 (m/s)	$Re \times 10^4$	$M = U_0/a$
1	0.02	32	4.238	0.093
2	0.02	48	6.358	0.140
3	0.02	49	6.490	0.143
4	0.02	55	7.285	0.160
5	0.02	64	8.477	0.186
6	0.02	67	8.874	0.195
7	0.03	32	6.357	0.093
8	0.03	48	9.536	0.140
9	0.03	49	9.735	0.143
10	0.03	55	10.927	0.160
11	0.03	64	12.715	0.186
12	0.03	67	13.311	0.195

References

- [1] V. Strouhal, Über eine besondere Art der Tonerregung, *Annalen der Physik und Chemie (Leipzig) Series 3* (5) (1878) 216–251.
- [2] L. Rayleigh, Aeroacoustical observations II, *Philosophical Magazine* 7 (1879) 149–162.
- [3] E.Y. Yudin, On the vortex sound from rotating rods, *Zhurnal Tekhnicheskoi Fizik* 14 (1944) 561 (English version, 1947, NACA TM 1136).
- [4] J.S. Cox, K.S. Brentner, C.L. Rumsey, Computation of vortex shedding and radiated sound for a circular cylinder: subcritical to transcritical Reynolds numbers, *Theoretical and Computational Fluid Dynamics* 12 (1998) 233–253.
- [5] F. Pérot, J.M. Auger, H. Giardi, C. Bailly, D. Juve, Computation of the noise generated by low Mach number flows around a cylinder and a wall-mounted half cylinder, *10th AIAA/CEAS Aeroacoustics Conference*, 2004.
- [6] X. Gloerfelt, F. Pérot, C. Bailly, D. Juvé, Flow-induced cylinder noise formulated as a diffraction problem for low Mach numbers, *Journal of Sound and Vibration* 287 (2005) 129–151.
- [7] A. Tosh, A. Frendi, Sh. Girimaji, Prediction of noise radiated by flow over a smooth square cylinder, *10th AIAA-Aeroacoustics Conference* 2004-2914, 2004.
- [8] O. Inoue, W. Iwakami, N. Hatakeyama, Aeolian tones from flow past two square cylinders in a side-by-side arrangement, *Physics of Fluids* 98 (2006) 046104.
- [9] W.F. King, E. Pfizenmaier, M. Herrmann, Aeroacoustical investigations of a full scale DSA-350 SEK pantograph in an anechoic free jet wind tunnel, DLR-IB 92517-96B4, 1996.
- [10] W.F. King, E. Pfizenmaier, M. Herrmann, On abating aerodynamic sound generated by components of high speed pantographs, DLR-IB 92517-96B9, 1996.
- [11] L.M. Jenkins, M.R. Khorrami, M.M. Choudhari, C.B. Mc Ginley, Characterization of unsteady flow structures around tandem cylinders for component interaction studies in airframe noise, *11th AIAA/CEAS Aeroacoustics Conference, AIAA 2005-2812*, 2005.
- [12] N.K. Delany, N.E. Sorensen, *Low-Speed Drag of Cylinders of Various Shapes*, NACA-TN 3038, 1953.
- [13] R. King, A review of vortex shedding research and its applications, *Ocean Engineering* 4 (1977) 141–171.
- [14] Dj. Farivar, Turbulent uniform flow around cylinders of finite length, *AIAA Journal* 19 (1981) 275–281.
- [15] V.J. Modi, A.K. Dikshit, Near-wakes of elliptic cylinders in subcritical flow, *AIAA Journal* 13 (1975) 490–497.
- [16] V.J. Modi, E. Wiland, Unsteady aerodynamics of stationary elliptic cylinders in subcritical flow, *AIAA Journal* 8 (1970) 1814–1821.
- [17] W.F. King III, Radiated aerodynamic noise generated by high-speed tracked vehicles, TRB Report No. 1475, Transportation Research Board, Washington, DC, USA, 1995, pp. 59–65.
- [18] W.F. King III, E. Pfizenmaier, M. Herrmann, L. Neuhaus, An experimental study of sound generated by flow interactions with cylinders, DLR-IB 92517-96/B11, part I: text, part II: figures, 1996.